MOX–Report No. 53/2012

An efficient XFEM approximation of Darcy flows in fractured porous media

Fumagalli, A.; Scotti, A.

MOX, Dipartimento di Matematica "F. Brioschi"
Politecnico di Milano, Via Bonardi 9 - 20133 Milano (Italy)

mox@mate.polimi.it http://mox.polimi.it

An efficient XFEM approximation of Darcy flows in fractured porous media

Alessio Fumagalli[♯] Anna Scotti[♯]

December 10, 2012

[♯] MOX– Modellistica e Calcolo Scientifico
Dipartimento di Matematica "F. Brioschi"
Politecnico di Milano
via Bonardi 9, 20133 Milano, Italy
alessio.fumagalli@mail.polimi.it
anna.scotti@mail.polimi.it

Keywords: Multiphase Darcy flow, fractured porous media, XFEM.

AMS Subject Classification: 05A16, 65N38, 78M50

Abstract

Subsurface flows are strongly influenced by the presence of faults and large fractures that alter the permeability of the medium acting as barriers or conduits for the flow. An accurate description of the hydraulic properties of the fractures is thus essential for the modelling of oil migration or the exploitation of unconventional sources. However, the width of fractures is often small compared to the typical mesh size. To approximate the problem without refining the mesh to resolve the fracture we replace them with surfaces immersed in the porous matrix. Moreover we allow the surfaces to be non matching with the edges of the grid handling the discontinuities within elements with the XFEM approach. The method, originally developed for the single-phase Darcy problem is extended to the case of passive transport and multiphase flow.

1 Introduction

Subsurface flows are strongly influenced by the presence of fractures. While small and microfractures can be easily accounted for by means of a simple homogenization resulting in an increase of permeability, large fractures and faults play a more complex role, acting as paths of barriers for the flow and connecting different regions of the domain. These effects are very relevant for many

applications such as oil migration, oil recovery, CO_2 storage and groundwater contamination and remediation.
Due to the spatial scales involved the simulation of fractured porous media is a very challenging task. The typical size of these features, compared to the domain size, is usually such that a very fine mesh is needed to resolve the fracture width. Moreover, in realistic cases, the porous media are usually crossed by a large number of fractures that can intersect each other. This geometric complexity makes the simulation of the flow in fractured porous media very challenging. If we consider the finite element method on an unstructured tetrahedral grid the construction of a good computational grid is essential to achieve accurate results. However, the conformity of the grid to possibly numerous and intersecting fractures can be a strong constraint and can affect the quality of the elements. Besides, the mesh refinement required to capture the fault or fracture aperture leads to a very high, if not unaffordable, computational cost.
These problems can be in part overcome with the model reduction strategy proposed in [1, 11] and later extended in [3]. It consists in a domain decomposition approach where the fractures are regarded as $n-1$ dimensional interfaces inside a n-dimensional porous matrix, *i.e.* surfaces in $3D$ or lines in $2D$. This approach can effectively reduce the number of unknowns in simulations because it removes the need for fine grids inside the fractures [7]. However, the aforementioned works are restricted to the case of grids that follow the shape of faults and fractures. In [5] the authors remove the constraint of mesh conformity by means of the extended finite element method (XFEM) [9], allowing the fracture to cross the elements of the grid in an arbitrary way. This approach has reduced the effort in constructing the computational grid, since this operation does not have to account for the possibly complicated geometry of the fractures and, moreover, can be performed only once even if the position of fractures or faults changes due to multiple scenarios or sensitivity analysis. The method was, however, limited to the case of one interface, or at most, of more non intersecting interfaces [7]. The difficulty in dealing with intersecting fractures is twofold. On one hand suitable coupling conditions have to be introduced at the intersections between two or more fractures. Furthermore, in an XFEM approach, the elements of the mesh that are crossed by more that one interface require an additional enrichment of the finite element space. Realistic simulations of intersecting faults in a three dimensional domain are presented in [2], where the continuity of pressure and mass conservation are enforced at the intersections. More general coupling conditions are introduced and discussed in [6] to account for different properties of the fractures allowing for pressure and velocity jumps at the intersection, similarly to the conditions derived in [11] for the matrix-fracture system. The aforementioned work considers the case of a network isolated by the porous matrix, in the limit case where the matrix can be regarded as impermeable with respect to the fractures. In the present paper we present discretization strategy for the fully coupled problem of porous media crossed by intersecting fractures, where the fractures exchange fluid between each other (we limit ourselves to the

intersections of two fractures at a time), and with the porous matrix surrounding them. To obtain a method that is as flexible as possible, in the view of future realistic applications, we employ the XFEM on two levels. First of all, we allow the grid of the medium to be non-conforming with the fractures. Moreover, we allow the grids of the fractures to be arbitrary, *i.e.* non-matching at the intersection, and handle the pressure and velocity jumps at the intersection points with $n-1$ dimensional extended finite elements, as done in [6]. A particular attention is devoted to the enrichment of the finite element spaces in the elements crossed by two fractures, where we extend the method proposed by [8] to allow the solution to be discontinuous across the two interfaces.
The paper is structured as follows: in Section 2 we present both the physical equations and the reduced model, with the interface conditions which couple the matrix-fracture system and the fracture-fracture system. In section 3 we present also the numerical discretization of the problem with an highlight on the enrichment of the finite element spaces. In Section 4 we present some numerical experiments to asses the effectiveness of the proposed method. Finally Section 5 is devoted to conclusions and to ongoing works.

2 Mathematical model

We call fracture, or fault, a thin zone of the porous medium with data different several order of magnitude from the neighbour medium, however its extension is comparable with the domain size. In the analyses we consider only the case of two intersecting fractures with only one intersection region. Nevertheless the results presented can be extended, rather easily and under the forthcoming hypotheses, to the case of several fractures with several intersections. Examples can be found in Section 4.

2.1 Physical equations

Let us consider a domain $D \in \mathbb{R}^2$, crossed by two intersecting fractures called $\Omega_1, \Omega_2 \in D$. Here and in the sequel we indicate with the lower case subscript $\cdot_i$ the restriction of data and unknowns to Ω_i. We assume that the intersecting region, called $\mathcal{I} := \Omega_1 \cap \Omega_2$, form a connected subset of each Ω_i, *i.e.* we allow only one intersection between the fractures. For simplicity we assume that $\mathcal{I}$ can be approximated by a quadrilateral with parallel sides. Given $\mathcal{I}$ each fracture Ω_i can be written as the union of disjoint sets $\Omega_i = \Omega_{i1} \cup \mathcal{I} \cup \Omega_{i2}$, the two non-empty branches Ω_{ij} of the fracture and the intersecting region. We indicate with $\cdot_{ij}$ and $\cdot_{\mathcal{I}}$ the restriction of data and unknowns to Ω_{ij} and to $\mathcal{I}$, respectively. Finally, thanks to the previous splitting of D, we define the surrounding porous medium to the fractures as $\Omega := D \setminus (\Omega_1 \cup \Omega_2)$. Figure 1 shows an example of the domain subdivision.
We divide the boundary of each fracture Ω_i into three disjoint pieces $\gamma_{i,1}$, $\gamma_{i,2}$ and a part common with ∂D, as Figure 1 shows.

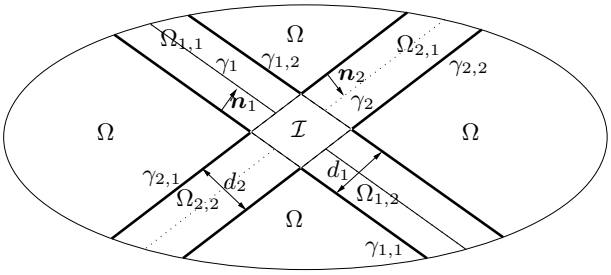

Figure 1: Example of the set subdivision for a given problem.

Following [6, 11] we introduce the thickness d_i of Ω_i, which is a regular function of the centre line γ_i of Ω_i. We can write each fracture Ω_i from its thickness as

$$\Omega_i = \left\{ \boldsymbol{x} \in \mathbb{R}^2 : \boldsymbol{x} = \boldsymbol{s} + r\boldsymbol{n}_i,\ \boldsymbol{s} \in \gamma_i,\ r \in \left(-\frac{d_i(\boldsymbol{s})}{2}, \frac{d_i(\boldsymbol{s})}{2} \right) \right\},$$

where we have indicated with $\boldsymbol{n}_i$ the inward, respect to Ω_i, unit normal to $\gamma_{i,1}$. We are interested in computing the steady pressure field p and the velocity field $\boldsymbol{u}$ in the whole domain D, which are governed by the Darcy problem formulated in Ω, Ω_1, Ω_2 and $\mathcal{I}$ as

$$\begin{cases} \boldsymbol{K}_j^{-1}\boldsymbol{u}_j + \nabla p_j = \boldsymbol{0} \\ \nabla\cdot \boldsymbol{u}_j = f_j \end{cases} \text{ in } \Omega_j \text{ for } j = \_, 1, 2 \quad \begin{cases} \boldsymbol{K}_{\mathcal{I}}^{-1}\boldsymbol{u}_{\mathcal{I}} + \nabla p_{\mathcal{I}} = \boldsymbol{0} \\ \nabla\cdot \boldsymbol{u}_{\mathcal{I}} = f_{\mathcal{I}} \end{cases} \text{ in } \mathcal{I}. \quad \text{(1a)}$$

Where $\boldsymbol{K}_j$ and $\boldsymbol{K}_{\mathcal{I}}$ denote the, symmetric and positive definite, permeability tensors and f_j and $f_{\mathcal{I}}$ source terms. To couple all the problems in (1a) we use the classical interface conditions

$$\begin{cases} p_i = p \\ \boldsymbol{u}_i \cdot \boldsymbol{n}_i = \boldsymbol{u} \cdot \boldsymbol{n}_i \end{cases} \text{ on } \partial\gamma_{i,j} \quad \text{and} \quad \begin{cases} p_i = p_I \\ \boldsymbol{u}_i \cdot \boldsymbol{n}_{\mathcal{I}} = \boldsymbol{u}_I \cdot \boldsymbol{n}_{\mathcal{I}} \end{cases} \text{ on } \partial\mathcal{I} \quad \text{(1b)}$$

for $i, j = 1, 2$. In (1b) we have indicated with $\boldsymbol{n}_{\mathcal{I}}$ the outward, respect to $\mathcal{I}$, unit normal. Finally we impose, for the sake of simplicity, homogeneous boundary condition on the pressure

$$\begin{cases} p = 0 & \text{on } \partial D \cap \partial\Omega, \\ p_i = 0 & \text{on } \partial D \cap \partial\Omega_i. \end{cases} \quad \text{(1c)}$$

Following [4] we can prove that problem (1) is well posed.

2.2 Reduced model

In [11] a reduced model is derived for a single fracture coupled with the porous media, while in [6] a similar model is derived for networks of fractures uncoupled with the surrounding porous medium. We present a reduced model, based on

the aforementioned works, which describe the coupling between a network of fractures and the porous medium obtaining a complete model for a single phase flow in fractured porous media.

We recall, for readers convenience, the main idea for both models. We start by collapsing each Ω_i with its centre line γ_i. Given a regular function $a : \Omega \to \mathbb{R}^m$, $m = 1$ or 2, let us set the jump and mean operators as $[\![a]\!]_\gamma := a_1 - a_2$ and $\{\!\{a\}\!\}_\gamma := (a_1 + a_2)/2$ with $a_j(\boldsymbol{x}) = \lim_{\epsilon \to 0^\pm} a(\boldsymbol{x} - \epsilon \boldsymbol{n})$. We define the same operators across the intersection point $\boldsymbol{i}_p := \gamma_1 \cap \gamma_2$ as $[\![a_i]\!]_{\boldsymbol{i}_p} := a_{i1} - a_{i2}$ and $\{\!\{a_i\}\!\}_{\boldsymbol{i}_p} := (a_{i1} + a_{i2})/2$ for $i = 1, 2$. We define the projection matrix on the normal space as $\boldsymbol{N}_i := \boldsymbol{n}_i \otimes \boldsymbol{n}_i$ and on the tangential space as $\boldsymbol{T}_i := \boldsymbol{I} - \boldsymbol{N}_i$. Given a regular function $a : \Omega_i \to \mathbb{R}$ the tangential operators, equal in this bi-dimensional case, are $\nabla_{\boldsymbol{\tau}_i} a := \boldsymbol{T}_i \nabla a$ and $\nabla_{\boldsymbol{\tau}_i} \cdot a := \boldsymbol{T}_i : \nabla a$. Following [6, 11] we suppose that $\boldsymbol{K}_i = K_{i,\boldsymbol{n}} \boldsymbol{N}_i + K_{i,\boldsymbol{\tau}} \boldsymbol{T}_i$ in $\Omega_i \setminus \mathcal{I}$ with $K_{i,\cdot}$ positive, while $\boldsymbol{K}_\mathcal{I}$ is constant. We will indicate with $\hat{\cdot}$ the reduced variables defined in each γ_i. We introduce, for each fracture γ_i, the reduced velocity $\hat{\boldsymbol{u}}_i$ and pressure $\hat{p}_i$ as

$$\hat{\boldsymbol{u}}_i(\boldsymbol{s}_i) := \int_{-\frac{d_i}{2}}^{\frac{d_i}{2}} \boldsymbol{T}_i \boldsymbol{u}_i(\boldsymbol{s}_i + r\boldsymbol{n}_i)\, dr \quad \text{and} \quad \hat{p}_i(\boldsymbol{s}_i) := \frac{1}{d_i} \int_{-\frac{d_i}{2}}^{\frac{d_i}{2}} p_i(\boldsymbol{s}_i + r\boldsymbol{n}_i)\, dr,$$

with $\boldsymbol{s}_i \in \gamma_i$. Moreover, the reduced source term $\hat{f}_i$ and the inverse of the scaled permeabilities η_{γ_i} and $\hat{\eta}_i$ are defined as

$$\hat{f}_i(\boldsymbol{s}_i) := \int_{-\frac{d_i}{2}}^{\frac{d_i}{2}} f_i(\boldsymbol{s}_i + r\boldsymbol{n}_i)\, dr, \quad \eta_{\gamma_i} := \frac{d_i}{K_{i,\boldsymbol{n}}} \quad \text{and} \quad \hat{\eta}_i := \frac{1}{d_i K_{i,\boldsymbol{\tau}}}.$$

Following [6] we indicate with $\boldsymbol{\tau}_i$ the tangential unit vector to γ_i, and with $\boldsymbol{\tau}_{i,\boldsymbol{i}_p}$ its value at $\boldsymbol{i}_p$. We define $d_i^* := d_i / \sin\theta$, with θ the angle between the two fractures at $\boldsymbol{i}_p$. The reduction process approximate the pressure in the intersecting region to a scalar value $\hat{p}_\mathcal{I}$ in $\boldsymbol{i}_p$. The latter and the reduced source term $f_\mathcal{I}$ are defined as

$$\hat{p}_\mathcal{I} := \frac{1}{|\mathcal{I}|} \int_\mathcal{I} p_\mathcal{I}(\boldsymbol{x})\, d\boldsymbol{x} \quad \text{and} \quad \hat{f}_\mathcal{I} := \frac{1}{|\mathcal{I}|} \int_\mathcal{I} f_\mathcal{I}(\boldsymbol{x})\, d\boldsymbol{x}.$$

Moreover we indicate the inverse of the reduced permeability, along the directions $\boldsymbol{\tau}_{i,\boldsymbol{i}_p}$ and $\boldsymbol{\tau}_{j,\boldsymbol{i}_p}$, in the intersection as $\eta_{ij}^\mathcal{I} := \boldsymbol{\tau}_{i,\boldsymbol{i}_p}^\top \cdot \boldsymbol{K}_\mathcal{I}^{-1} \boldsymbol{\tau}_{j,\boldsymbol{i}_p}$.

The complete reduced model describe the evolution of $\boldsymbol{u}$, p, $\hat{\boldsymbol{u}}_i$, $\hat{p}_i$ and $\hat{p}_\mathcal{I}$ using the following system of partial differential equations for $i = 1, 2$

$$\begin{cases} \boldsymbol{K}^{-1}\boldsymbol{u} + \nabla p = \boldsymbol{0} & \text{in } \Omega \\ \nabla \cdot \boldsymbol{u} = f & \\ p = 0 & \text{on } \partial D \cap \partial\Omega \end{cases} \qquad \begin{cases} \hat{\eta}_i \hat{\boldsymbol{u}}_i + \nabla_{\boldsymbol{\tau}_i} \hat{p}_i = \boldsymbol{0} & \\ \nabla_{\boldsymbol{\tau}_i} \cdot \hat{\boldsymbol{u}}_i = \hat{f}_i + [\![\boldsymbol{u} \cdot \boldsymbol{n}_i]\!]_{\gamma_i} & \text{in } \gamma_i \setminus \boldsymbol{i}_p \\ \hat{p}_i = 0 & \text{on } \partial\gamma_i \end{cases} \tag{2a}$$

coupled with the interface conditions for the matrix-fracture system for $j = 1, 2$

$$\begin{cases} \xi_{0i} \eta_{\gamma_i} [\![\boldsymbol{u} \cdot \boldsymbol{n}_i]\!]_{\gamma_i} = \{\!\{p\}\!\}_{\gamma_i} - \hat{p}_i \\ \eta_{\gamma_i} \{\!\{\boldsymbol{u} \cdot \boldsymbol{n}_i\}\!\}_{\gamma_i} = [\![p]\!]_{\gamma_i} \end{cases} \quad \text{on } \gamma_i, \tag{2b}$$

with $\xi_{0j} \in (0, 0.25]$ a first model parameter, see [3, 11] for its meaning. Moreover the coupling conditions for the fracture-fracture system for $i \neq j = 1, 2$ are

$$\begin{cases} \sum_{k=1}^{2} [\![\hat{\boldsymbol{u}}_k \cdot \boldsymbol{\tau}_k]\!]_{\boldsymbol{i}_p} = \hat{f}_{\mathcal{I}} \\ \frac{|\mathcal{I}|}{d_i} \sum_{k=1}^{2} \frac{\eta_{ik}^{\mathcal{I}}}{d_k^*} \{\!\{ \hat{\boldsymbol{u}}_k \cdot \boldsymbol{\tau}_k \}\!\}_{\boldsymbol{i}_p} = [\![\hat{p}_i]\!]_{\boldsymbol{i}_p} \\ \hat{\xi}_0 \frac{d_j}{d_i} \eta_{ii}^{\mathcal{I}} [\![\hat{\boldsymbol{u}}_i \cdot \boldsymbol{\tau}_i]\!]_{\boldsymbol{i}_p} = \{\!\{ \hat{p}_i \}\!\}_{\boldsymbol{i}_p} - \hat{p}_{\mathcal{I}} \end{cases} \quad \text{in } \boldsymbol{i}_p. \tag{2c}$$

The value of the second model parameter $\hat{\xi}_0$ is discussed in [6].

3 Numerical discretization

The discretization of (2) is based on the XFEM method [9] for both the porous medium and the intersecting fractures. In fact we allow non-matching grids between the fractures and the porous media and in the intersection point of the intersecting fractures. To this purpose we introduce suitable enriched finite element spaces based on the standard Raviart-Thomas finite element $\mathbb{RT}_0$, for vector fields, and piecewise constant finite element $\mathbb{P}_0$, for scalar fields.
We consider a family of regular tessellation $\mathcal{T}_h$, $h := \max_{K \in \mathcal{T}_h} \operatorname{diam}(K)$, with $\partial\mathcal{T}_h := \{e \in \partial K,\ K \in \mathcal{T}_h\}$. For each fracture i we introduce a family of regular tessellation $\gamma_{\hat{h},i}$ with $\hat{h} := \max_{l \in \gamma_{\hat{h},i}} |l|$. We suppose that if a fracture intersect a triangle then it intersects exactly two edges moreover, for the sake of simplicity, we suppose that at most two fractures cross a triangle and, if an intersection occurs, it happens inside a triangle. We introduce the following subset of $\mathcal{T}_h$, for $i \neq j$ and for $i, j = 1, 2$

$$\begin{aligned} \mathcal{I}_h &:= \{K \in \mathcal{T}_h :\ (\gamma_i \cap \gamma_j \neq \emptyset) \in K\}, \\ \mathcal{M}_h &:= \{K \in \mathcal{T}_h :\ K \cap (\gamma_i \cup \gamma_j) \neq \emptyset\} \setminus \mathcal{I}_h, \\ \mathcal{G}_{h,i} &:= \{K \in \mathcal{T}_h :\ K \cap \gamma_i \neq \emptyset \wedge K \cap \gamma_j = \emptyset\}, \\ \mathcal{CR}_h := \mathcal{M}_h \cup \mathcal{I}_h \cup \mathcal{G}_{h,1} \cup \mathcal{G}_{h,2} \quad &\text{and} \quad \mathcal{N}_h := \mathcal{T}_h \setminus \mathcal{CR}_h. \end{aligned}$$

The last two are the cut region and the collection of elements in $\mathcal{T}_h$ not crossed by any fracture, respectively. We split also the mesh of the fractures into intersected elements and non intersected elements, in particular we define for $i = 1, 2$

$$\mathcal{C}_{\hat{h},i} := \left\{ l \in \gamma_{\hat{h},i} :\ l \cap \boldsymbol{i}_p \neq \emptyset \right\} \quad \text{and} \quad \mathcal{B}_{\hat{h},i} := \gamma_{\hat{h},i} \setminus \mathcal{C}_{\hat{h},i}.$$

See Figure 2 for an example. With this subdivision, we define the following

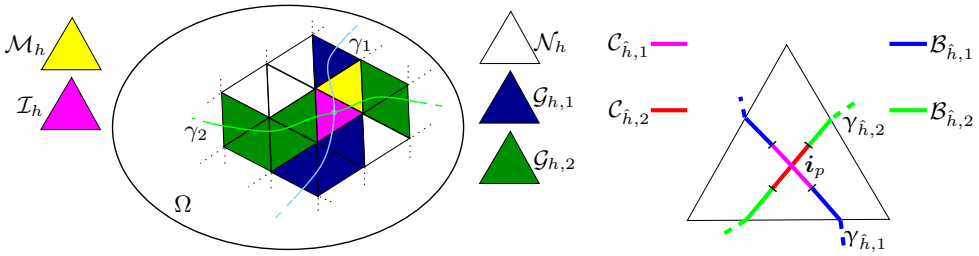

Figure 2: Example of subdivision of $\mathcal{T}_h$, in the left, and $\gamma_{\hat{h},i}$, in the right.

enriched finite elements spaces for the medium

$$\widetilde{\mathbb{RT}}_0(\mathcal{T}_h) := \mathbb{RT}_0(\mathcal{N}_h) \oplus \bigcup_{k,j=1}^{2} \mathbb{RT}_0(\mathcal{G}_{h,k}) \oplus \bigcup_{m=1}^{3} \mathbb{RT}_0(\mathcal{M}_h) \oplus \bigcup_{l=1}^{4} \mathbb{RT}_0(\mathcal{I}_h),$$

$$\widetilde{\mathbb{P}}_0(\mathcal{T}_h) := \mathbb{P}_0(\mathcal{N}_h) \oplus \bigcup_{k,j=1}^{2} \mathbb{P}_0(\mathcal{G}_{h,k}) \oplus \bigcup_{m=1}^{3} \mathbb{P}_0(\mathcal{M}_h) \oplus \bigcup_{l=1}^{4} \mathbb{P}_0(\mathcal{I}_h).$$

With these definitions we can represent, for both p and $\boldsymbol{u}$, four discontinuities in $K \in \mathcal{I}_h$, two in $K \in \mathcal{M}_h$ and one in $K \in \mathcal{G}_{h,k}$. An example is reported in Figure 3.

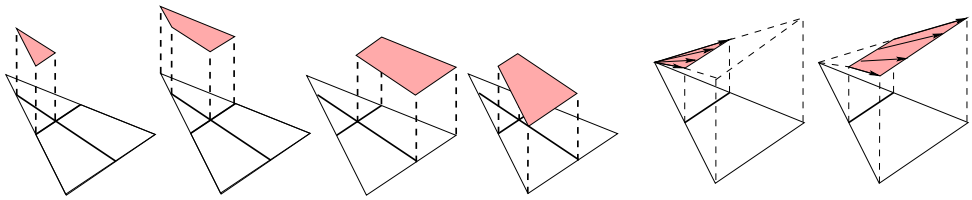

(a) Example of $\mathbb{P}_0(\mathcal{I})$.

(b) Example of $\mathbb{RT}_0(\mathcal{G}_h)$.

Figure 3: Example of some base functions for cut elements.

Moreover for each fracture $i = 1, 2$ the enriched finite elements spaces are

$$\widetilde{\mathbb{RT}}_0\left(\gamma_{\hat{h},i}\right) := \mathbb{RT}_0\left(\mathcal{B}_{\hat{h},i}\right) \oplus \bigcup_{k=1}^{2} \mathbb{RT}_0\left(\mathcal{C}_{\hat{h},i}\right),$$

$$\widetilde{\mathbb{P}}_0\left(\gamma_{\hat{h},i}\right) := \mathbb{P}_0\left(\mathcal{B}_{\hat{h},i}\right) \oplus \bigcup_{k=1}^{2} \mathbb{P}_0\left(\mathcal{C}_{\hat{h},i}\right).$$

Using a standard procedure we can write problem 2 in its discrete counterpart, see [5, 6] for more details. Hence the global algebraic system is the following

symmetric saddle problem

$$\begin{bmatrix} \boldsymbol{A} & \boldsymbol{B} & \boldsymbol{0} & \boldsymbol{E}_1 & \boldsymbol{0} & \boldsymbol{E}_2 & \boldsymbol{0} \\ \boldsymbol{B}^\top & \boldsymbol{0} & \boldsymbol{0} & \boldsymbol{0} & \boldsymbol{0} & \boldsymbol{0} & \boldsymbol{0} \\ \boldsymbol{0} & \boldsymbol{0} & \hat{\boldsymbol{A}}_1 & \hat{\boldsymbol{B}}_1 & \boldsymbol{0} & \boldsymbol{0} & \hat{\boldsymbol{E}}_1 \\ \boldsymbol{E}_1^\top & \boldsymbol{0} & \hat{\boldsymbol{B}}_1^\top & \boldsymbol{0} & \boldsymbol{0} & \boldsymbol{0} & \boldsymbol{0} \\ \boldsymbol{0} & \boldsymbol{0} & \boldsymbol{0} & \boldsymbol{0} & \hat{\boldsymbol{A}}_2 & \hat{\boldsymbol{B}}_2 & \hat{\boldsymbol{E}}_2 \\ \boldsymbol{E}_2^\top & \boldsymbol{0} & \boldsymbol{0} & \boldsymbol{0} & \hat{\boldsymbol{B}}_2^\top & \boldsymbol{0} & \boldsymbol{0} \\ \boldsymbol{0} & \boldsymbol{0} & \hat{\boldsymbol{E}}_2^\top & \boldsymbol{0} & \hat{\boldsymbol{E}}_2^\top & \boldsymbol{0} & \boldsymbol{0} \end{bmatrix} \begin{bmatrix} \boldsymbol{u} \\ p \\ \hat{\boldsymbol{u}}_1 \\ \hat{p}_1 \\ \hat{\boldsymbol{u}}_2 \\ \hat{p}_2 \\ \hat{p}_\mathcal{I} \end{bmatrix} = \begin{bmatrix} \boldsymbol{0} \\ \boldsymbol{F}_q \\ \boldsymbol{0} \\ \hat{\boldsymbol{F}}_1 \\ \boldsymbol{0} \\ \hat{\boldsymbol{F}}_2 \\ \hat{\boldsymbol{F}}_\mathcal{I} \end{bmatrix}.$$

The matrices $\boldsymbol{E}_i$ and $\hat{\boldsymbol{E}}_i$ are the interpolations matrices, for the pressure, between the matrix-fracture system and the fracture-fracture system.

4 Applicative examples

We present some examples and test cases to asses the reduced model presented in Section 2.2. Example 4.1 highlight the model error using the reduced method instead the physical equations, while Example 4.2 shows a synthetic test case.

4.1 Model error

The model error is the error we commit if we use the reduced model (2) instead of solving the real equations (1). We define the error err as the difference between a reference solution, obtained using the original equations solved on a fine grid, and the reduced solution; moreover we introduce also the relative error as

$$err := \|p - p_{ref}\|_{L^2(\Omega)} \quad \text{and} \quad err_{rel} := \frac{err}{\|p_{ref}\|_{L^2(\Omega)}}. \tag{3}$$

We consider a two-dimensional problem in a square domain cut by two intersecting fractures characterized by different properties, let us set $\Omega = (0,\, 1)^2$,

$$\gamma_1 = \{(x, y) \in \Omega :\ y = 0.387\} \quad \text{and} \quad \gamma_2 = \{(x, y) \in \Omega :\ y = -2x + 1.4\}.$$

In the boundaries for the domain $\partial\Omega$ and for each fracture $\partial\gamma_i$, for $i = 1, 2$, we prescribe homogeneous natural boundary conditions. The bulk flow and the flow in the intersecting fractures are described by (2) with source terms $f = 10$ and $\hat{f}_i = 10d$ for both fractures and $\boldsymbol{K} = \boldsymbol{I}$, with d the thickness of the fracture. Fracture γ_1 is characterized by the same tangential and normal permeability as the porous medium in Ω thus $\hat{\eta}_1 = d^{-1}$ and $\eta_{\gamma_1} = d$. Fracture γ_2 is instead characterized by the same tangential permeability as the porous medium in Ω *i.e.* $\hat{\eta}_2 = d^{-1}$, and a low normal permeability $\eta_{\gamma_2} = 50d$. We set $\hat{\xi}_0 = 0$. The computational domain is sketched in Figure 6.
Figure 4 shows the pressure field in the domain Ω and in the fractures γ_1 and γ_2, with and without the reduced model. Due to the small normal permeability

of γ_2 there is a jump in the pressure across this fracture, furthermore the effect of fracture γ_1 is null since it has the same permeability tensor as the porous matrix.

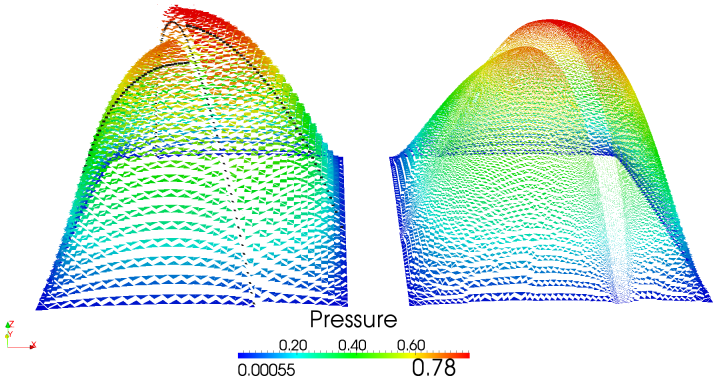

Figure 4: On the left the solution with the reduced model, with $\xi_0 = 0.25$ and $d = 0.02$, using 4418 triangles for the medium, 101 segments for first fracture and 102 segments for the second fractures. On the right the reference solution with 114115 triangles.

In Table 1 the global relative error (3) defined in 1 is reported.

	$\xi_0 = 0$	$\xi_0 = 0.25$	$\xi_0 = 0.5$
$d = 0.02$	0.0437599	0.0440597	0.0456497
$d = 0.05$	0.072244	0.0726848	0.0724751

Table 1: Global relative error err_{rel} for different values of thickness d and shape parameter ξ_0.

We notice that decreasing the thickness d of the fracture the model error decreases, while changing the shape parameter ξ_0 the model error does not change significantly.
Figure 5 shows the model error (3) considering the global domain and the domain without the first fracture. We take as a reference the solution of the real problem with a fine grid composed by 114115 triangles. Due to the model reduction the major errors are localized near the fractures, in particular when a pressure jump occurs across a fracture.
In Figure 6 we present a zoom of the error near the intersection point $\boldsymbol{i}_p$, we can notice that the error is comparable with the neighbouring regions.

4.2 A synthetic test case

Let us consider a synthetic test case that aims at reproducing the quarter of five spots problem in the presence of fractures. The computational domain is the unit square and no flux boundary conditions are imposed on the edges. The

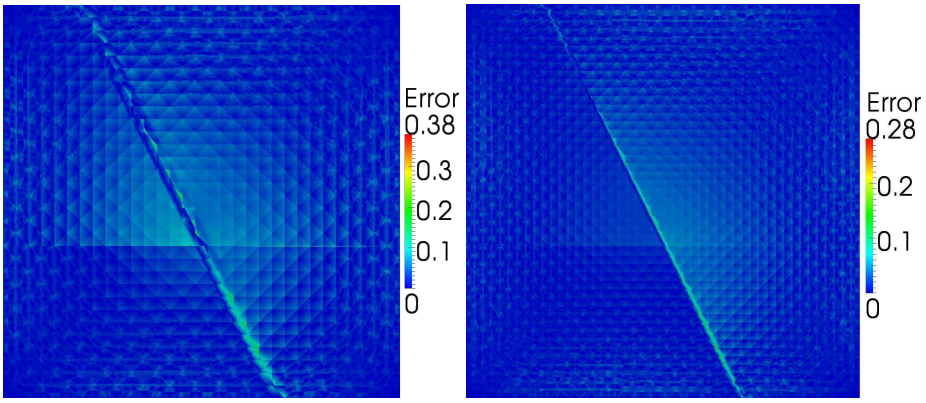

Figure 5: On the left image the model error (3) for thickness $d = 0.05$ while on the right image the model error (3) for thickness $d = 0.02$. In both simulation the shape parameter is $\xi_0 = 0.25$.

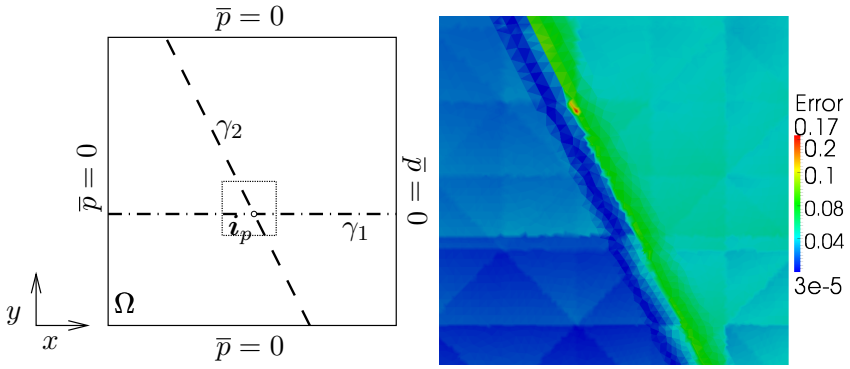

Figure 6: On the left image the zoom, coloured in green, of the domain Ω while on the right image the zoom of the model error for thickness $d = 0.02$, with shape parameter $\xi_0 = 0.25$.

presence of the injector well at the left bottom corner and the extracting well at the top right corner is mimicked with two source terms of equal intensity and opposite sign, *i.e.*

$$f = \begin{cases} 1 & \text{if } x^2 + y^2 < 0.08 \\ -1 & \text{if } (1-x)^2 + (1-y)^2 < 0.08 \\ 0 & \text{otherwise} \end{cases}.$$

The geometry of the fracture replicates one of the test cases proposed in [10] and there solved with the finite volume method on a grid conforming to the

fractures. In particular we have three fractures,

$$\gamma_1 : y = 0.20 \leq x \leq 0.6$$
$$\gamma_2 : x = 0.30 \leq y \leq 0.4$$
$$\gamma_3 : x = 0.70.3 \leq x \leq 0.7$$

of the same width $d = 0.01$ and permeability $K_{i,\boldsymbol{n}} = K_{i,\boldsymbol{\tau}} = 100$ for $i = 1, 2, 3$, while the permeability of the porous matrix is set to 1. The solution is reported in Figure 7, where the pressure distribution is obviously influenced by the presence of the fractures. The zoom of the intersection region close to the injector shows that the fractures can cut the triangles of the mesh, and, moreover, the grids of the fracture are independent on each other and also on the two-dimensional mesh. Figure 8 compares the isolines of pressure in the non fractured and fractured case, highlighting the effect of the higher conductivity due to the fractures.

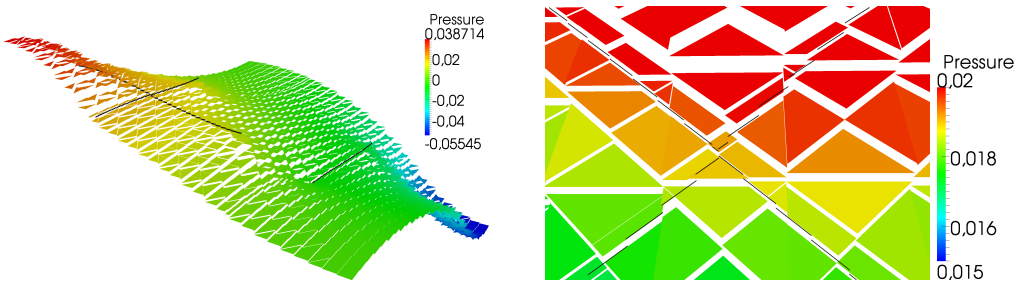

Figure 7: Pressure distribution for a "quarter of five spots" configuration in the presence of three intersecting and highly permeable fratures. On the right, zoom of the intersection showing the non conformity of the 2D and 1D grids.

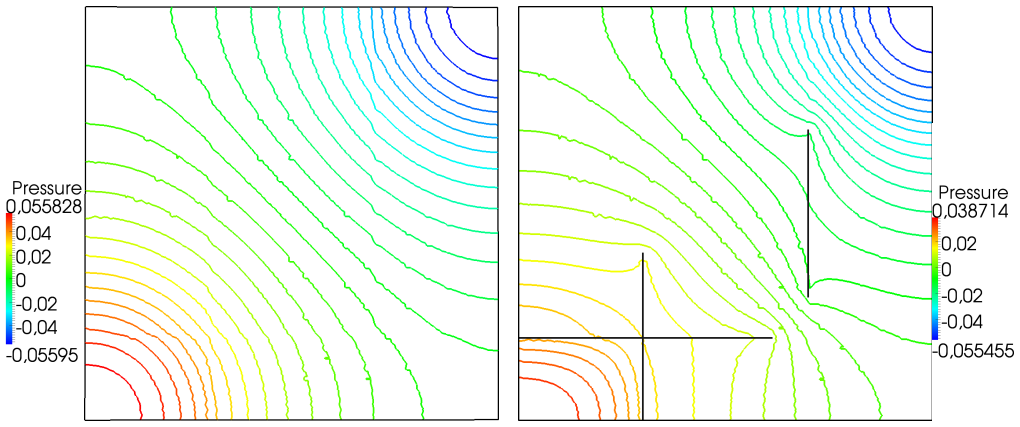

Figure 8: Plot of the pressure isolines in the absence (left) and in the presence (right) of three intersecting and highly permeable fratures.

5 Conclusions

In this paper we have proposed a numerical method for the numerical approximation of Darcy problems in fractured porous media. The main original aspect with respect to the methods already present in literature is the use of the XFEM to represent discontinuous velocity and pressure across the fractures also in the case of intersecting fracture. We assessed the validity of this approach comparing its results with those computed with the standard mixed finite element on a grid fine enough to resolve the fracture thickness. The solutions were in good agreement, except for the error introduced by the use of the reduced one-dimensional model for the fractures, that vanishes if the fracture aperture tends to zero. Moreover, the choice of the new coupling conditions introduced in [6] for intersecting fractures allowed us to represent more general configurations such as the simultaneous presence of blocking and conductive fractures. Even if the method has been, so far, implemented only in the two-dimensional case where the fractures are represented as lines, it can already have an applicative interest for instance for the simulation of fractured reservoirs with numerical upscaling techniques. The development of the corresponding three dimensional method is the subject of ongoing and future work.

6 Acknowledgments

The research has been financed by Eni e&p Division. The second author also acknowledges the support of MIUR through the PRIN09 project n. 2009Y4RC3B 001. The authors wish to thank Luca Formaggia, Jérôme Jaffré and Jean Roberts for many fruitful discussions.

References

[1] C. Alboin et al. "Domain decomposition for some transmission problems in flow in porous media". In: *Numerical treatment of multiphase flows in porous media (Beijing, 1999)*. Vol. 552. 2000, pp. 22–34.

[2] L. Amir, M. Kern, V. Martin, and J. E. R. Roberts. "Décomposition de domaine et préconditionnement pour un modèle 3D en milieu poreux fracturé". In: *Proceeding of JANO 8, 8th conference on Numerical Analysis and Optimization*. 2005.

[3] P. Angot, F. Boyer, and F. Hubert. "Asymptotic and numerical modelling of flows in fractured porous media". In: *M2AN Math. Model. Numer. Anal.* 43.2 (2009), pp. 239–275.

[4] F. Brezzi and M. Fortin. *Mixed and Hybrid Finite Element Methods*. Vol. 15. Springer Verlag, Berlin, 1991.

[5] C. D'Angelo and A. Scotti. "A mixed finite element method for Darcy flow in fractured porous media with non-matching grids". In: *Mathematical Modelling and Numerical Analysis* 46.02 (2012), pp. 465–489.

[6] L. Formaggia, A. Fumagalli, A. Scotti, and P. Ruffo. "A reduced model for Darcy's problem in networks of fractures". 2012.

[7] A. Fumagalli and A. Scotti. "Numerical modelling of multiphase subsurface flow in the presence of fractures". In: *Communications in Applied and Industrial Mathematics* (2011). In press.

[8] A. Hansbo and P. Hansbo. "An unfitted finite element method, based on Nitsche's method, for elliptic interface problems". In: *Comput. Methods Appl. Mech. Engrg.* 191.47-48 (2002), pp. 5537–5552.

[9] P. Hansbo. "Nitsche's method for interface problems in computational mechanics". In: *GAMM-Mitt.* 28.2 (2005), pp. 183–206.

[10] M. Karimi-Fard, L. Durlofsky, and K. Aziz. "An Efficient Discrete-Fracture Model Applicable for General-Purpose Reservoir Simulators". In: *SPE Journal* 9.2 (2004), pp. 227–236.

[11] V. Martin, J. Jaffré, and J. E. Roberts. "Modeling fractures and barriers as interfaces for flow in porous media". In: *SIAM J. Sci. Comput.* 26.5 (2005), pp. 1667–1691.

MOX Technical Reports, last issues

Dipartimento di Matematica "F. Brioschi",
Politecnico di Milano, Via Bonardi 9 - 20133 Milano (Italy)

53/2012 Fumagalli, A.; Scotti, A.
An efficient XFEM approximation of Darcy flows in fractured porous media

52/2012 Perotto, S.
Hierarchical model (Hi-Mod) reduction in non-rectilinear domains

51/2012 Beck, J.; Nobile, F.; Tamellini, L.; Tempone, R.
A quasi-optimal sparse grids procedure for groundwater flows

50/2012 Carcano, S.; Bonaventura, L.; Neri, A.; Esposti Ongaro, T.
A second order accurate numerical model for multiphase underexpanded volcanic jets

49/2012 Migliorati, G.;Nobile, F.;von Schwerin, E.;Tempone, R.
Approximation of Quantities of Interest in stochastic PDEs by the random discrete L2 projection on polynomial spaces

48/2012 Ghiglietti, A.; Paganoni, A.M.
Statistical properties of two-color randomly reinforced urn design targeting fixed allocations

47/2012 Astorino, M.; Chouly, F.; Quarteroni, A.
Multiscale coupling of finite element and lattice Boltzmann methods for time dependent problems

46/2012 Dassi, F.; Perotto, S.; Formaggia, L.; Ruffo, P.
Efficient geometric reconstruction of complex geological structures

45/2012 Negri, F.; Rozza, G.; Manzoni, A.; Quarteroni, A.
Reduced basis method for parametrized elliptic optimal control problems

43/2012 Secchi, P.; Vantini, S.; Vitelli, V.
A Case Study on Spatially Dependent Functional Data: the Analysis of Mobile Network Data for the Metropolitan Area of Milan